Hydrocarbon lakes on Titan: Distribution and interaction with a porous regolith

A. Hayes,[1] O. Aharonson,[1] P. Callahan,[2] C. Elachi,[2] Y. Gim,[2] R. Kirk,[3] K. Lewis,[1] R. Lopes,[2] R. Lorenz,[4] J. Lunine,[5] K. Mitchell,[2] G. Mitri,[2] E. Stofan,[6] and S. Wall[2]

Received 24 January 2008; revised 26 March 2008; accepted 31 March 2008; published 14 May 2008.

[1] Synthetic Aperture Radar (SAR) images of Titan's north polar region reveal quasi-circular to complex features which are interpreted to be liquid hydrocarbon lakes. We investigate methane transport in Titan's hydrologic cycle using the global distribution of lake features. As of May 2007, the SAR data set covers ~22% of the surface and indicates multiple lake morphologies which are correlated across the polar region. Lakes are limited to latitudes above 55°N and vary from <10 to more than 100,000 km^2. The size and location of lakes provide constraints on parameters associated with subsurface transport. Using porous media properties inferred from Huygens probe observations, timescales for flow into and out of observed lakes are shown to be in the tens of years, similar to seasonal cycles. Derived timescales are compared to the time between collocated SAR observations in order to consider the role of subsurface transport in Titan's hydrologic cycle. **Citation:** Hayes, A., et al. (2008), Hydrocarbon lakes on Titan: Distribution and interaction with a porous regolith, *Geophys. Res. Lett.*, *35*, L09204, doi:10.1029/2008GL033409.

1. Introduction

[2] Recent results from Cassini have suggested the presence of liquid hydrocarbons in Titan's northern latitudes and the presence of a liquid-bearing porous medium near its equator [*Stofan et al.*, 2007; *Lorenz and Lunine*, 2006]. Analogous to water on Earth, surface conditions on Titan are near the triple point of methane, suggesting a methane-based hydrologic cycle which may incorporate solid, liquid, and gaseous phases. Observations of hydrologic features can be used to investigate transport in Titan's methane cycle through atmospheric evaporation [*Mitri et al.*, 2007], surface flow, and sub-surface drainage. In this work, we describe the interaction between a porous medium and the potential hydrocarbon lakes discovered by Cassini.

2. Lake Distribution in the North Polar Region

[3] The K_u band Radar (2.17 cm wavelength) on the Cassini spacecraft is a multi-mode (imaging, altimetry, radiometry, and scatterometry) instrument designed to penetrate Titan's optically opaque atmosphere. When operating in imaging mode, high resolution (300–720 m/pixel with a cross-track range of 120–460 km) is obtained by applying Synthetic Aperture Radar (SAR) processing to the echo bursts [*Elachi et al.*, 2004].

[4] The first hydrocarbon lake features were identified in July 2006 and reported by *Stofan et al.* [2007]. The backscatter cross-sections in the dark patches are low compared to their surroundings, suggesting a smooth surface at a scale of 2 cm. Radiometric brightness differences are consistent with a flat surface with low dielectric constant, such as liquid hydrocarbons, surrounded by a water ice regolith [*Stofan et al.*, 2007]. We have identified 655 lake features in SAR data from 7 Titan flybys between July 2006 and May 2007. Observed lake features are confined to latitudes above 55°N, where 55.4% of the surface has been observed. Global SAR coverage (as of May 2007) encompasses 22.4% of the surface, 2.4% of which is covered by lakes. Overlapping swath sections, which cover 27.1% of coverage above 55°N, can be used to study temporal variation in observed features.

2.1. Mapping Unit Distribution

[5] Lake-like features are separated into 3 classes; dark lakes, granular lakes, and bright lakes (see Figures 1b–1d). Dark lakes are seen above 65°N, where they take up 15% of the observed surface area. Granular lakes are distinguished from dark lakes by a relative increase in backscatter, although there is no distinct transition between these two units (see Figure 1a). Bright lakes are morphologically similar to dark and granular lakes, but have an interior with equal or higher backscatter than their immediate surroundings. Dark lakes are interpreted as liquid filled while bright lakes are interpreted as empty basins. Based on backscatter and location, granular lakes are inferred as transitional between dark and bright lake features. Superpositions of these units are also observed. Figure 2 shows the spatial distribution of mapping units.

[6] Dark lakes account for 394 of the 655 mapped lake features and 84% of the area of all lake units. The areal distribution of dark lakes is approximately log normal with a mean of 87 km^2. Lakes with areas in excess of 10^4 km^2 represent 73% of the dark lake area and are generally confined to a region between 0°E and 140°E. For mapping purposes, dark lakes are defined as having ratios between median incidence-angle-corrected backscatter cross-sections inside and immediately outside the feature of $\leq$0.6. There is a trend toward lower ratios with increasing latitude (Figure 1a), suggesting radiation is either better reflected (specular) or absorbed by lakes closer to the pole. This

[1]Division of Geological and Planetary Sciences, California Institute of Technology, Pasadena, California, USA.
[2]Jet Propulsion Laboratory, California Institute of Technology, Pasadena, California, USA.
[3]U.S. Geological Survey, Flagstaff, Arizona, USA.
[4]Johns Hopkins University Applied Physics Laboratory, Laurel, Maryland, USA.
[5]Lunar and Planetary Laboratory, University of Arizona, Tucson, Arizona, USA.
[6]Proxemy Research, Laytonsville, Maryland, USA.

0094-8276/08/2008GL033409$05.00

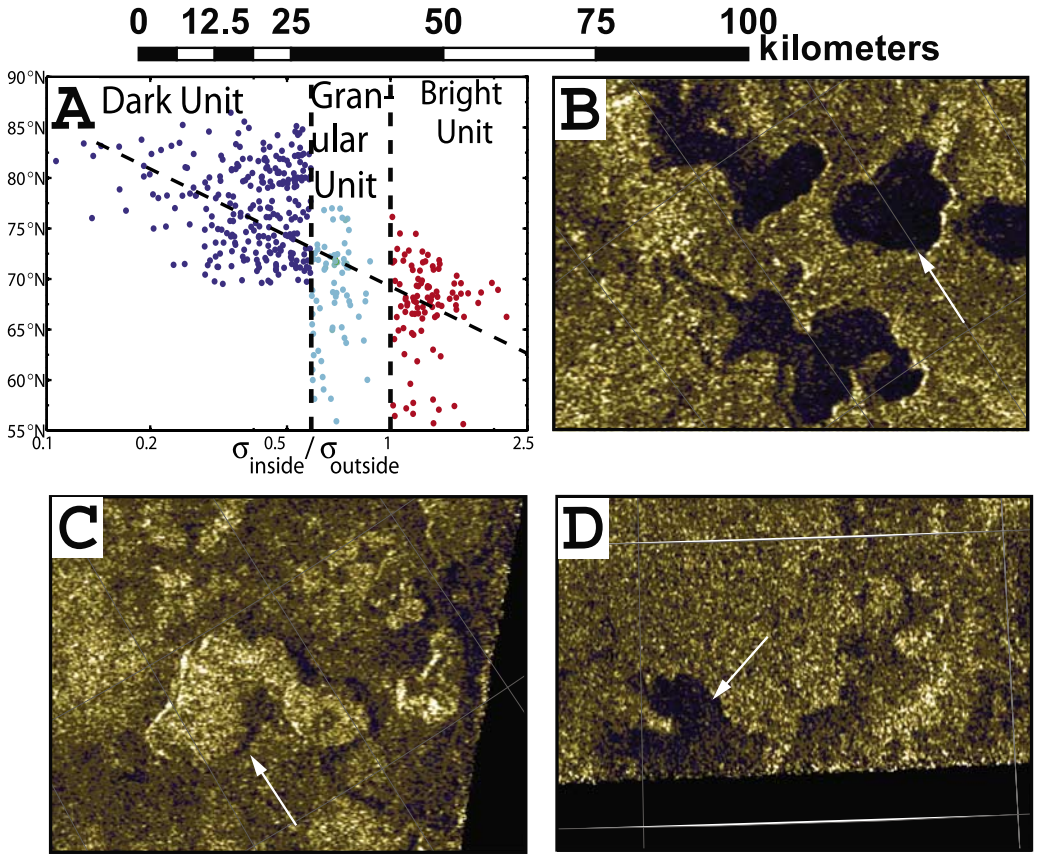

Figure 1. Mapping Units: (a) Ratio between median incidence-angle-corrected off-axis backscatter within and immediately surrounding feature, (b) Dark Unit, (c) Bright Unit, and (d) Granular Unit.

behavior is expected if lakes are deeper at higher latitudes. Granular lakes, defined as having backscatter ratios between 0.6 and 1.0, represent a smooth transition from dark lakes. Bright lakes, which have ratios $\geq$1, show distinct separation from granular lakes in backscatter ratio.

[7] Granular lakes are found below 77°N and represent 6% of the total mapped lake area. The latitudinal emergence of granular lakes coincides with that of bright lake features. In almost all areas of Titan granular lakes are found in close proximity to bright lakes, suggesting an evolutionary relationship. Granular lakes show an increase in non-uniformity and relative backscatter ratio, consistent with radiation penetrating a liquid layer and interacting with the lake bottom. A histogram of the 109 granular lake areas is approximately log normal with a mean of 147 km^2.

[8] Bright lakes are interpreted as 200–300 m deep empty basins. 152 bright lakes have been mapped and represent 10% of lake features. The areal distribution of bright lakes, which is also log normal, has a mean of 273 km^2. The increase in characteristic area between dark, granular, and bright lakes may be related to the balance between evaporation and subsurface transport (see Section 3).

[9] During the May 2007 flyby, altimetry data, coincident with previous SAR swaths, were obtained during closest approach. Figure 3 shows the position of the altimetry footprints on top of SAR imagery. The footprints coincide with two bright lake features. Surface heights are reported as the centroid of the altimetry waveforms and confirm that the bright lakes are depressions with 200–300 m walls. The sloping nature of the lake profile is a byproduct of topographic averaging within altimetry footprints. The integration of received power within an altimetry echo is proportional to nadir backscatter cross-section. For each bright lake the interior is brighter than the surroundings in both off-axis and nadir backscatter, suggesting that the radar-bright nature of empty lakes is compositional or due to volume scattering effects, as opposed to differences in roughness at 2 cm. A liquid-filled lake would be expected to have high nadir and low off-axis backscatter.

2.2. Morphology

[10] The morphology of lakes on Titan span the range of observed morphologies on Earth. Lakes with distinctly polygonal shapes, rough shoreline geometries, and associated channels are similar to terrestrial drainage lakes dominated by surface flow. Comparatively rounded lake boundaries with sharp shorelines and no associated channel networks are consistent with seepage lakes interacting with a local ground-methane system. Other lakes seem to be dendritic or branching in nature and have similar morphology to flooded river valleys [*Stofan et al.*, 2007]. Observed lakes appear to be in varying states of evolution, ranging from slightly under-filled (dark/granular lakes) to completely empty (bright lakes). Granular and bright lakes are not seen above 77°N and are almost always found within close proximity of each other. A notable exception is between 180°E and 240°E, where bright lakes are found in the absence of granular lakes. This region is also characterized

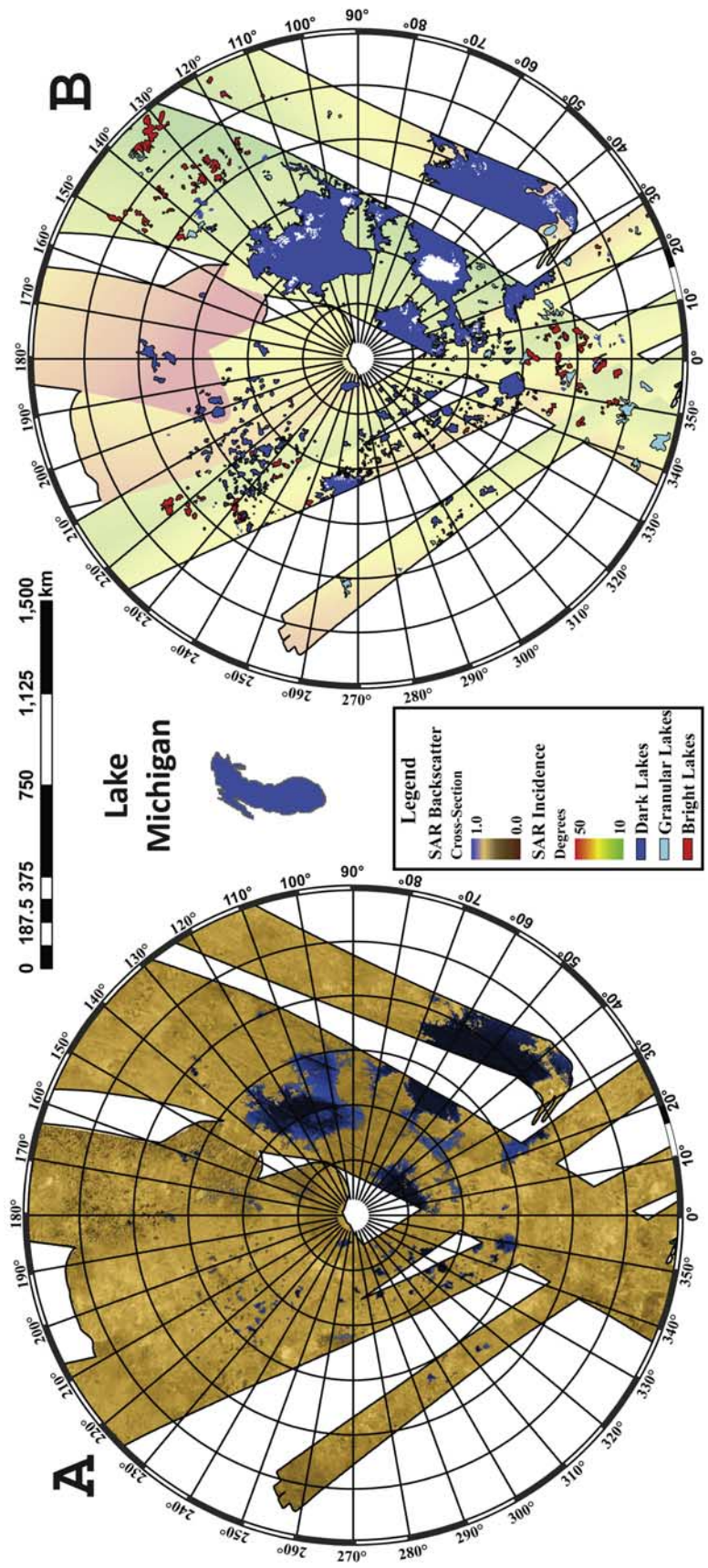

Figure 2. Distribution of lake features above 60°N: (a) Mosaic of Cassini SAR swaths through May 2007. (b) Distribution of mapping units. Dark lakes are blue, granular lakes are cyan, and bright lakes are red. Background color represents incidence angle during acquisition. Note outline of Lake Michigan for relative scale.

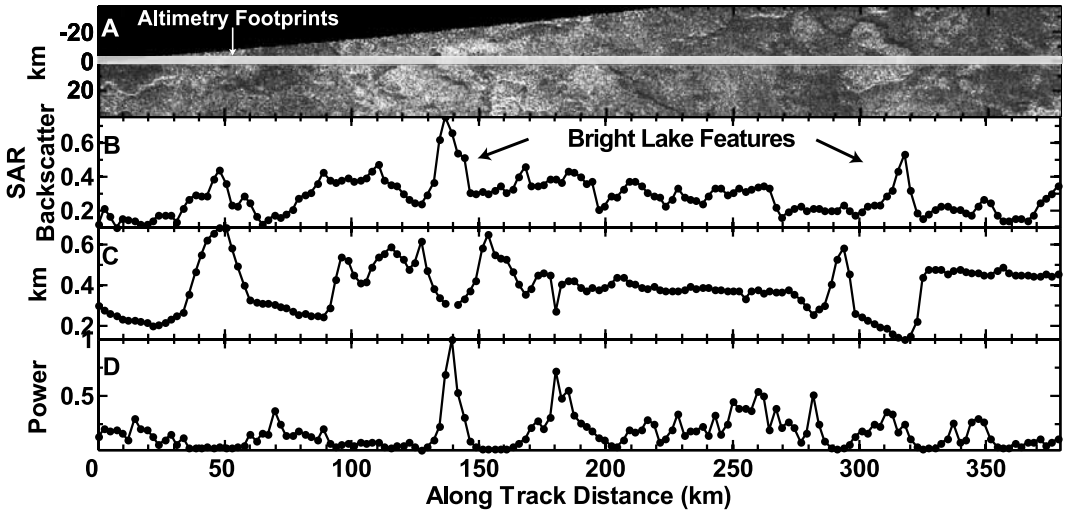

Figure 3. (a) SAR backscatter with altimetry footprints overlain, (b) median SAR backscatter within altimetry footprints, (c) centroid of altimetry waveforms (average height above 2575 km), and (d) integrated altimetry waveform power (normalized), which is proportional to nadir backscatter. Note correlated peaks/dips at ~140 and ~320 km corresponding to bright lake features.

by a large density of small circular features consistent with a network of seepage lakes (K. Mitchell et al., Titan's north polar lake district: Insights from the Cassini titan radar mapper, manuscript in preparation, 2008) interacting with a subsurface alkanofer, i.e. the analog of an aquifer on Earth.

3. Flow Through Porous Media

[11] The rate of liquid inflow or outflow from a lake through the subsurface is governed by regional topography and the properties of the local porous medium. The Huygens Probe provided information constraining soil properties near (168°E, 10°S) and suggested the presence of a damp porous medium consisting of loosely packed particles between the sizes of silt to medium sand [*Lorenz and Lunine*, 2006; *Zarnecki et al.*, 2005]. The material properties observed by Huygens are used as a starting point to model subsurface transport in Titan's northern latitudes. Flow is assumed to be primarily horizontal and approximately described by a one dimensional form of the groundwater flow equation in cylindrical geometry, known as the Boussinesq equation:

$$\frac{\partial h}{\partial t} = \frac{1}{\phi r}\frac{\partial}{\partial r}\left(Krh\frac{\partial h}{\partial r}\right) + E, \qquad (1)$$

where h is the height of the alkanofer surface, t is time, ϕ is porosity, r is distance from the lake center, and K is the hydraulic conductivity ($K = \kappa\rho g/\mu$). Hydraulic conductivity, which describes the ability of liquid to flow through pore space, depends on the permeability of the porous medium (κ), liquid density (ρ), gravity (g), and dynamic viscosity (μ). Permeability can vary by up to 6 orders of magnitude for the grain sizes observed by Huygens. For simplicity, flow is modeled using methane as the primary constituent and results are investigated for a significant range of permeabilities: 10^{-4} (medium sand) to 10^{-10} (silt) cm^2.

[12] Equation (1) is modified from its standard form only in the addition of an evaporation rate, E. The evaporation rate is taken to be 0.3 m/yr, consistent with an average surface wind speed of 0.1 m/s, methane mixing ratio of 0.35 in the lakes, and methane relative humidity (RH) of 50% [*Tomasko et al.*, 2005], although RH is likely greater because of a 2-3 K temperature drop between the equator and poles. Evaporation rates are derived by balancing latent and sensible heat fluxes, as in the work by *Mitri et al.* [2007], and depend linearly on surface wind speed, methane mixing ratio, and deviation from saturation (1-RH). A wind speed of 0.1 m/s is consistent with the lack of observed wave activity on lake surfaces and cooling rates of the Huygens probe [*Lorenz*, 2006]. Vertical infiltration is characteristically 2 orders of magnitude faster than horizontal seepage and is approximated by the hydraulic conductivity. Complete vertical infiltration would occur on a timescale of $\sim H/K$, where H is the lake depth and K varies from 1 to 10^6 m/yr for the permeability range mentioned above ($\kappa = 10^{-6}$ cm^2 corresponds to $K = 10^4$ m/yr). To date, none of the lakes observed by coincident swaths have displayed shoreline change, suggesting that a methane table or impermeable boundary exists within a distance of H/ϕ from the bottom of the lake and that subsurface flow is predominantly horizontal. However, additional observations may reveal change resulting from vertical infiltration.

[13] Permeability can be a strong function of length scale; dominated by the porous medium over small scales and cracks and caverns over large scales. For the purposes of this work, permeability is assumed homogeneous and isotropic. Hydraulic conductivity is usually anisotropic and flows tend to partially disperse horizontally and refract vertically at contacts in horizontally graded soils. In the absence of crustal stirring, non-volatile products of photolysis, which settle down to Titan's surface [*Yung et al.*, 1984], may have formed a 10-100 m scale layer above a more permeable regolith derived from early meteoric bombardment.

[14] Figure 4 describes two end-members in a range of case studies investigating the interaction between a hydrocarbon lake and its surrounding porous medium. The first (Figure 4a) represents a lake, initially filled, with the

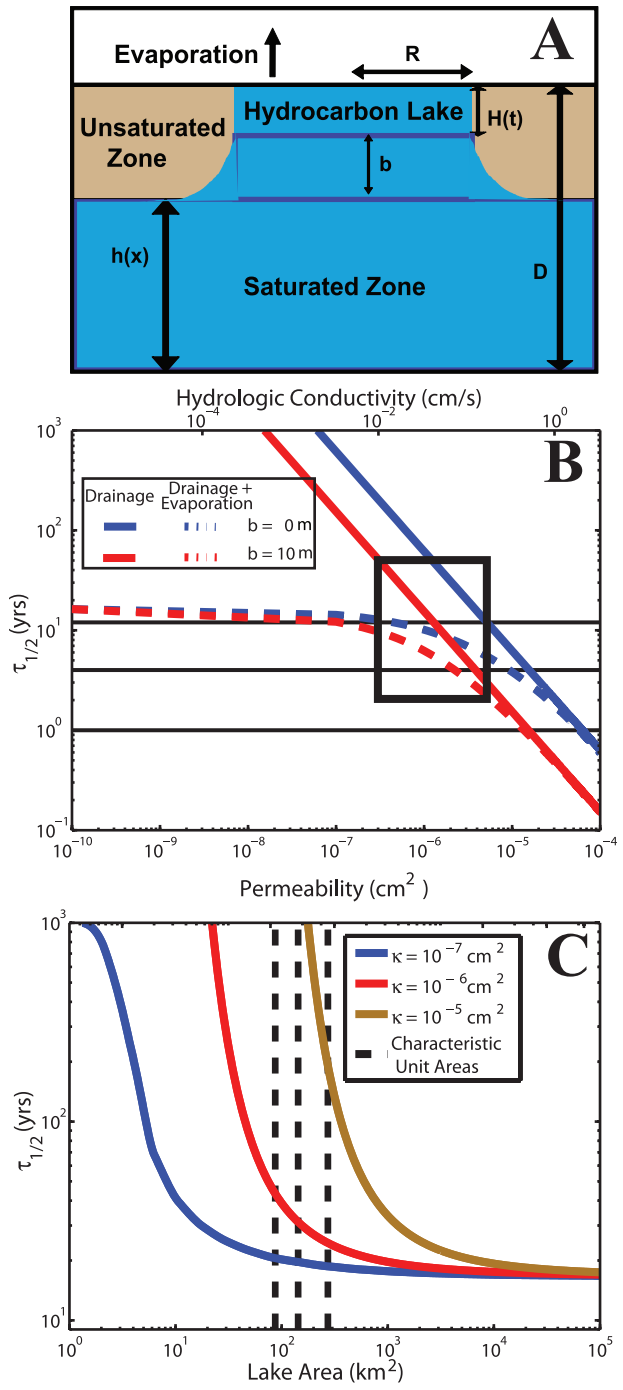

Figure 4. Interaction between a single lake and its immediate surroundings: (a) Model parameters. Lake resting in regolith with a saturated alkanofer a distance b from its bottom. $h = D$ when the alkanofer is coincident with the surface and $(D - h) \geq H$ when the lake is sitting in unsaturated regolith. (b) Drainage timescales for horizontal diffusion into an unsaturated regolith. Black lines represent the current overlap (~1 yr), nominal mission (~4 yrs), and maximum mission (~12 yrs) lengths. The highlighted region is the most probable permeability range based on Huygens data. (c) Removal timescale versus lake area when the methane table is coincident with the lake surface. Vertical lines are the characteristic areas of dark, granular, and bright lakes.

saturated zone existing a distance b beneath the lake bottom. The second case represents a lake coincident with the saturated zone, which can be created from Figure 4a by setting $h = D$. The temporal evolution of each system can be described by equation (1) using appropriate initial conditions and assuming no flow lines penetrate the saturated zone. The solutions shown in Figure 4 can be approximately scaled to varying initial conditions using:

$$\tau_{1/2} \sim \left[\pm \frac{4KH}{R^2} \left(\left(1 + \frac{b}{H} \right)^2 + \frac{SR}{H} \left(1 + \frac{b}{H} \right) \right) + \frac{2E}{H} \right]^{-1} \quad (2)$$

where S is the slope of the methane table and equation (2) is the harmonic average of characteristic timescales for evaporation and infiltration. The sign of the first term is determined by the direction of subsurface flow, positive for outflow and negative for inflow. In the case where the methane table is coincident with the lake surface, $b = 0$ and the first term is negative. Under the assumption that no flow lines penetrate into the saturated zone, subsurface loss is proportional to the area of the lake walls, while evaporative loss scales with surface area. Hence, the ratio of these fluxes scale with lake radius, the dominant loss term transitioning from subsurface transport for small lakes to evaporative loss for large lakes. Note that while evaporation will remove liquid methane, liquid ethane and nitrogen are comparatively stable at Titan's surface.

[15] The first case study (Figure 4a) is a simplified example of a drainage lake, which is emptied by both sub-surface transport and evaporation. When the methane table is located below the lake bottom, it is assumed that the liquid will vertically infiltrate to the level of the table, creating a cylindrical volume that will radially diffuse out of the regolith. Drainage timescales for 100 km^2 lakes (median dark lake size), located 0 and 10 m above the methane table are depicted in Figure 4b. A lake depth of 10 m is chosen [*Paillou et al.*, 2008]. For permeabilities $<10^{-6}$ cm^2, evaporation begins to dominate and drainage timescales are limited to of order 10 years, similar to seasonal timescales. The interpretation of this result is that disequilibrium conditions can persist over timescales exceeding 10 years for porous media properties consistent with Huygens probe observations. Drainage timescales for lakes located in highly permeable environments ($\kappa > 10^{-4}$ cm^2) are dominated by infiltration while impermeable environments ($\kappa < 10^{-7}$ cm^2) are dominated by evaporation.

[16] In the second case study, which represents an ideal seepage morphology, evaporation removes liquid methane while infiltration replenishes it until the local alkanofer is depleted. In Figure 4c, the dependance of area on removal timescales for a seepage dominated morphology is shown. For large lakes, evaporation dominates and removal timescales are similar to cases where the surrounding medium is unsaturated. For each permeability, however, there exists a size threshold below which influx from the regolith can balance evaporation in a quasi-stable state over multiple seasonal cycles. For the region consistent with a seepage morphology between 240°E and 180°E, where the dark lakes are ~100 km^2 and bright lakes are characteristically ~200 km^2, this suggests a permeability of order 10^{-5} or 10^{-6} cm^2 if we assume that equilibrium has been

reached. Repeat observations during the Cassini extended mission may help test this hypothesis.

4. Summary

[17] Lake size and distribution illuminate aspects of hydrologic activity in the north polar region of Titan. Dark lakes are found between 90°N and 70°N, showing a general trend of decreased off-axis backscatter moving poleward. Granular lakes emerge at ~77°N and are found as far South as 55°N. Backscatter ratio variation between dark and granular lakes suggest a smooth transition between the two classifications. Bright and granular lakes are found interspersed in the same latitude ranges. Integration of altimetry waveforms show that bright lakes are radar bright in both nadir and off-axis backscatter, suggesting they have similar roughness length scales to surrounding terrain but different material properties. Potential explanations include the collection of micron-sized atmospheric fallout particles or evaporative products into the lakes or mm to cm-scale porosity structures beneath the lake beds, possibly created by dissolution chemistry.

[18] The distribution and character of lake-like features can be used to constrain parameters associated with sub-surface flow. Basic case studies suggest that timescales for lake drainage are of order 10 years for permeabilities $<10^{-6}$ cm^2, similar to seasonal timescales. A region consistent with seepage morphology between 240 °E and 180° E suggests that permeabilities in the local area are of order 10^{-5} or 10^{-6} cm^2. Theoretical vertical seepage rates suggest that lake floors are within H/ϕ of the methane table or an impermeable boundary. Continued observations over the lifetime of the Cassini mission will place upper bounds on the effective permeability in the North polar region. If changes are observed, lower bounds can be estimated as well. Topographic information is currently being used to incorporate mapped lake distributions into sub-surface flow models and will be discussed in a future paper. This will allow the study of the interaction between the surface and subsurface and its role in generating observed morphologies.

[19] **Acknowledgments.** Work was performed with the Cassini RADAR Team. The authors would like to thank Tom Farr, Ronald Blom, and Michael Janssen of JPL and David Stevenson of Caltech for helpful discussions, and the Cassini engineering team, without whom the data presented here would not have been possible.

References

Elachi, C., et al. (2004), Radar: The Cassini Titan Radar Mapper, *Space Sci. Rev.*, *115*, 71–110, doi:10.1007/s11214-004-1438-9.

Lorenz, R. D. (2006), Thermal interactions of the Huygens probe with the Titan environment: Constraint on near-surface wind, *Icarus*, *182*, 559–566, doi:10.1016/j.icarus.2006.01.009.

Lorenz, R. D., and J. I. Lunine (2006), Titan's damp ground: Constraints on Titan's surface thermal properties from the temperature evolution of the Huygens GCMS inlet, *Meteorit. Planet. Sci.*, *41*, 1–10.

Mitri, G., A. P. Showman, J. I. Lunine, and R. D. Lorenz (2007), Hydrocarbon lakes on Titan, *Icarus*, *186*, 385–394, doi:10.1016/j.icarus.2006.09.004.

Paillou, P., K. Mitchell, S. Wall, G. Ruffié, C. Wood, R. Lorenz, E. Stofan, J. Lunine, R. Lopes, and P. Encrenaz (2008), Microwave dielectric constant of liquid hydrocarbons: Application to the depth estimation of Titan's lakes, *Geophys. Res. Lett.*, *35*, L05202, doi:10.1029/2007GL032515.

Stofan, E. R., et al. (2007), The lakes of Titan, *Nature*, *445*, 61–64, doi:10.1038/nature05438.

Tomasko, M. G., et al. (2005), Rain, winds and haze during the Huygens probe's descent to Titan's surface, *Nature*, *438*, 765–778, doi:10.1038/nature04126.

Yung, Y. L., M. Allen, J. P. Pinto (1984), Photochemistry of the atmosphere of Titan-Comparison between model and observations, *Astrophys. J.*, *55*, 465–506, doi:10.1086/190963.

Zarnecki, J. C., et al. (2005), A soft solid surface on Titan as revealed by the Huygens Surface Science Package, *Nature*, *438*, 792–795, doi:10.1038/nature04211.

O. Aharonson, A. Hayes, and K. Lewis, California Institute of Technology, MC 150-21, Pasadena, CA 91125, USA. (hayes@gps.caltech.edu)

P. Callahan, C. Elachi, Y. Gim, R. Lopes, K. Mitchell, G. Mitri, and S. Wall, Jet Propulsion Laboratory, California Institute of Technology, Pasadena, CA 91109, USA.

R. Kirk, U.S. Geological Survey, Flagstaff, AZ 86001, USA.

R. Lorenz, Johns Hopkins University Applied Physics Laboratory, Laurel, MD 20723, USA.

J. Lunine, Lunar and Planetary Laboratory, University of Arizona, Tucson, AZ 85721, USA.

E. Stofan, Proxemy Research, 20528 Farcroft Lane, Laytonsville, MD 20882, USA.